Overexpression of *NEUROG2* and *NEUROG1* in human embryonic stem cells produces a network of excitatory and inhibitory neurons

Congyi Lu,*,†,‡,§,1 Xi Shi,*,‡,1 Andrew Allen,* David Baez-Nieto,* Alexandria Nikish,¶ Neville E. Sanjana,†,§ and Jen Q. Pan*,2

*Stanley Center for Psychiatric Research, Broad Institute, Cambridge, Massachusetts, USA; †New York Genome Center, New York, New York, USA; ‡McGovern Institute for Brain Research and ¶Department of Biological Engineering, Massachusetts Institute of Technology (MIT), Cambridge, Massachusetts, USA; and §Department of Biology, New York University, New York, New York, USA

ABSTRACT: Overexpression of mouse neurogenin (*Neurog*)2 alone or in combination with mouse *Neurog2/1* in human embryonic stem cells (hESCs) and human induced pluripotent stem cells (hiPSCs) can rapidly produce high-yield excitatory neurons. Here, we report a detailed characterization of human neuronal networks induced by the expression of human *NEUROG2* together with human *NEUROG2/1* in hESCs using molecular, cellular, and electrophysiological measurements over 60 d after induction. Both excitatory synaptic transmission and network firing activity increased over time. Strikingly, inhibitory synaptic transmission and GABAergic cells were identified from *NEUROG2/1* induced neurons (iNs). To illustrate the application of such iNs, we demonstrated that the heterozygous knock out of *SCN2A*, whose loss-of-function mutation is strongly implicated in autism risk, led to a dramatic reduction in network activity in the *NEUROG2/1* iNs. Our findings not only extend our understanding of the *NEUROG2/1*-induced human neuronal network but also substantiate *NEUROG2/1* iNs as an *in vitro* system for modeling neuronal and functional deficits on a human genetic background.—Lu, C., Shi, X., Allen, A., Baez-Nieto, D., Nikish, A., Sanjana, N. E., Pan, J. Q. Overexpression of *NEUROG2* and *NEUROG1* in human embryonic stem cells produces a network of excitatory and inhibitory neurons. FASEB J. 33, 000–000 (2019). www.fasebj.org

KEY WORDS: neurogenin · induced neuronal network · GABAergic · *SCN2A*

One of the major challenges of studying human neurologic disorders is the lack of access to the affected neural tissue, which limits molecular and cellular examinations of pathogenesis. Although animal models are widely used and may capture certain neurologic phenotypes consistent with human diseases, they do not fully recapitulate complex human behaviors because of evolutionary divergence in brain circuits and structures. As a result, successes in ameliorating phenotypes in preclinical animal models often do not translate to clinical efficacy (1, 2). In addition, it is not practical to use animal models for large-scale screening assays. Some of these limitations may be addressed by using cultured human neurons in an appropriate genetic context relevant to human neurologic diseases.

Both human embryonic stem cells (hESCs) (3–5) and human induced pluripotent stem cells (hiPSCs) (6, 7) can be induced to differentiate into human neurons and serve as cellular resources for modeling neurologic disorders in the human genomic context. Several protocols have been developed and refined in recent years for induced neuron (iN) differentiation from hESCs/hiPSCs (8, 9). In 2013, Zhang *et al.* (8) reported that a single mouse transcription factor [mouse neurogenin (*Neurog*)2 or *Neurog1*] could efficiently convert hESCs and hiPSCs into functional excitatory neurons. In 2014, an independent study showed that overexpression of *Neurog2/1* in hiPSCs caused rapid neuronal differentiation (10). Recently, the electrical properties of iNs induced by *Neurog2/1* were further characterized over 2 mo of culture, supporting the glutamatergic nature of *Neurog2/1* iNs (11). Here, we established iNs induced by human *NEUROG2/1* from hESCs and performed a detailed characterization of their

molecular, cellular, and electrophysiological properties over 60 d after induction. We found that *NEUROG2/1* iNs can be easily maintained in culture and that their synaptic and firing activities robustly increased with development. Strikingly, we identified GABA-positive cells and inhibitory transmission later in development, indicating the development of a complex iN network with both excitatory and inhibitory neurotransmission, which has not been reported before for other neurogenin-induced neuronal differentiation strategies.

To explore the application of *NEUROG2/1* iNs, we evaluated the functional impact of disrupting *SCN2A* on such a network. *SCN2A* mutation has been shown to be associated with autism (12, 13), developmental delays (14) and infantile seizure disorders (15). We utilized clustered regularly interspaced short palindromic repeat (CRISPR)/CRISPR-associated protein 9 (Cas9) genome editing to produce hESCs with heterozygous loss of function (LOF) of *SCN2A* (16). Using the *NEUROG2/1* differentiation protocol, we found a dramatic reduction in network activity throughout the culture period in iNs with a heterozygous knock out of *SCN2A*. Our findings not only extend our understanding of the dynamic changes in *NEUROG2/1*-induced human neuronal networks but also demonstrate the utility of this system for modeling specific aspects of neurologic disorders in human neurons.

MATERIALS AND METHODS

Cell culture

The hESC line 66 (HUES66) was obtained from the Harvard Stem Cell Institute (Cambridge, MA, USA). As previously described (10), hESCs were plated in standard tissue culture dishes coated with Geltrex (A1413301; Thermo Fisher Scientific, Waltham, MA, USA) diluted 1:100 in DMEM (10566024; Thermo Fisher Scientific). The cells were dissociated by Accutase (07920; StemCell Technologies, Vancouver, BC, Canada) and maintained in mTeSR medium (05850; StemCell Technologies) in the presence of Normocin (Ant-nr-1; InvivoGen, San Diego, CA, USA) to reduce the risk of bacterial and mycoplasma contamination. Rho kinase inhibitor (Y-27632) (688001; Millipore Sigma, Burlington, MA, USA) was added to the mTeSR medium at a final concentration of 10 μM during subculture to increase the survival rate of single cells. Mouse glial cells were obtained from the cortex of wild-type B6/C57 postnatal day (P)0 mice. Cortices from P0 mice were cut into pieces and digested with papain for 30 min; the cells were dissociated by harsh trituration using a glass pipette and plated onto 10-cm cell culture dishes in DMEM supplemented with 10% fetal bovine serum. Upon reaching confluence, the glial cells were trypsinized and subcultured at a 1:5 dilution at least 3 times before being used for coculture with iNs.

Generation of iNs from hESCs

Lentiviral delivery was used to introduce constitutive expression of reverse tetracycline-controlled transactivator 3 driven by the human elongation factor-1α promoter and inducible expression of *NEUROG2/1* driven by a tetracycline response element promoter into hESCs. To select for cells expressing *NEUROG2/1*, a puromycin resistance gene encoding puromycin-N-acetyltransferase (also known as pac) was linked to *NEUROG2/1* by a porcine teschovirus-1 2A (P2A) linker (**Fig. 1A**). On d 0, the transduced hESCs were plated in the presence of doxycycline (1 μg/ml) (D3447; MilliporeSigma) in mTeSR medium. The cells were plated in Geltrex-coated 12-well Axion microelectrode array (MEA) plates (Axion Biosystems, Atlanta, GA, USA) at a density of 1×10^4/well for MEA recording or in 6-well cell culture plates at a density of 1×10^5/well for quantitative PCR (qPCR), immunocytochemistry (ICC), and patch-clamp recording. Glass coverslips (354087; Corning, Corning, NY, USA) were included in the 6-well cell culture plates for ICC and patch-clamp recording. The cells were selected in puromycin (1 μg/ml) from d 1 to 4 in mTeSR medium with gradually increasing neural basal (NB) medium (mTeSR to NB ratio: 3:1 on d 1, 1:1 on d 2, and 1:3 on d 4). On d 4, the puromycin was removed, and the culture medium was changed to 100% NB. Mouse glial cells (4×10^4 cells/well in a 12-well MEA plate or 4×10^5/well in a 6-well cell culture plate for ICC and patch-clamp recording) were added on d 5 to enhance neuron maturation. On d 7, Ara-C (C1768, 1 μM; MilliporeSigma) was added to control the growth of the glial cells. After d 7, 1/4 of the medium was replaced every 2–3 d. Doxycycline (1 μg/ml) was present throughout the entire culture period.

MEA recordings and data analysis

The electrical activity of iNs was recorded using the Axion MEA system (Axion Biosystems) with an integrated amplifier. Each MEA dish (M768-GLx; Axion Biosystems) contained 12 wells with 64 microelectrodes (Au, 30 μm diameter) arranged over an 8×8 square grid with a 200-μm center-to-center spacing in each well. The recordings started 5 min after the MEA plates were placed on the Maestro recording chamber, which was set to 35°C and supplied with a continuous perfusion of 5% carbon dioxide-balanced air (Airgas, Cambridge, MA, USA) throughout recording. For all time points, each MEA recording lasted 15 min. All MEA recordings were performed in the culture medium.

The electrical signals were collected at 10 kHz and analyzed offline using Axion's Integrated Studio software. Raw MEA data were first high-pass filtered at 200 Hz to remove low-frequency local field potentials. Spikes were detected using a threshold-based detector set to an upward or downward excursion beyond $6 \times$ SD above the peak-to-peak noise level. Spike sorting was not performed; multiunit activity may therefore contribute to the spikes that were detected from 1 electrode. The timestamps of the spikes were used for further analysis. The spike rate was calculated by dividing the total number of spikes by the recording time (15 min) per electrode. Electrodes without any spike activity were excluded from spike rate analysis. Raster plots were generated from timestamp data using Neuroexplorer (Madison, AL, USA). Cross correlations were calculated by comparing timestamp data collected from electrodes in the same MEA well with MatLab (MathWorks, Natick, MA, USA).

Patch-clamp recording

Coverslips with iNs were placed in the recording chamber on the stage of an inverted microscope (Axiovert.A1; Zeiss, Oberkochen, Germany) equipped with phase-contrast optics. All recordings were performed at room temperature (24°C–26°C). The continuously perfused extracellular solution contained (mM) 145 NaCl, 5 KCl, 1 $MgCl_2$, 2 $CaCl_2$, 5 4-(2-hydroxyethyl)-1-piperazineethanesulfonic acid (HEPES), and 5 glucose (all from MilliporeSigma), and the pH was adjusted to 7.4 with NaOH. Electrodes were pulled using a horizontal P-1000 pipette puller (Sutter Instrument, Novato, CA, USA). Membrane potentials were recorded in the current-clamp whole-cell configuration using pipettes filled with K-gluconate recording solution containing (mM) 131 K-gluconate, 17.5 KCl, 1 $MgCl_2$, 10 HEPES,
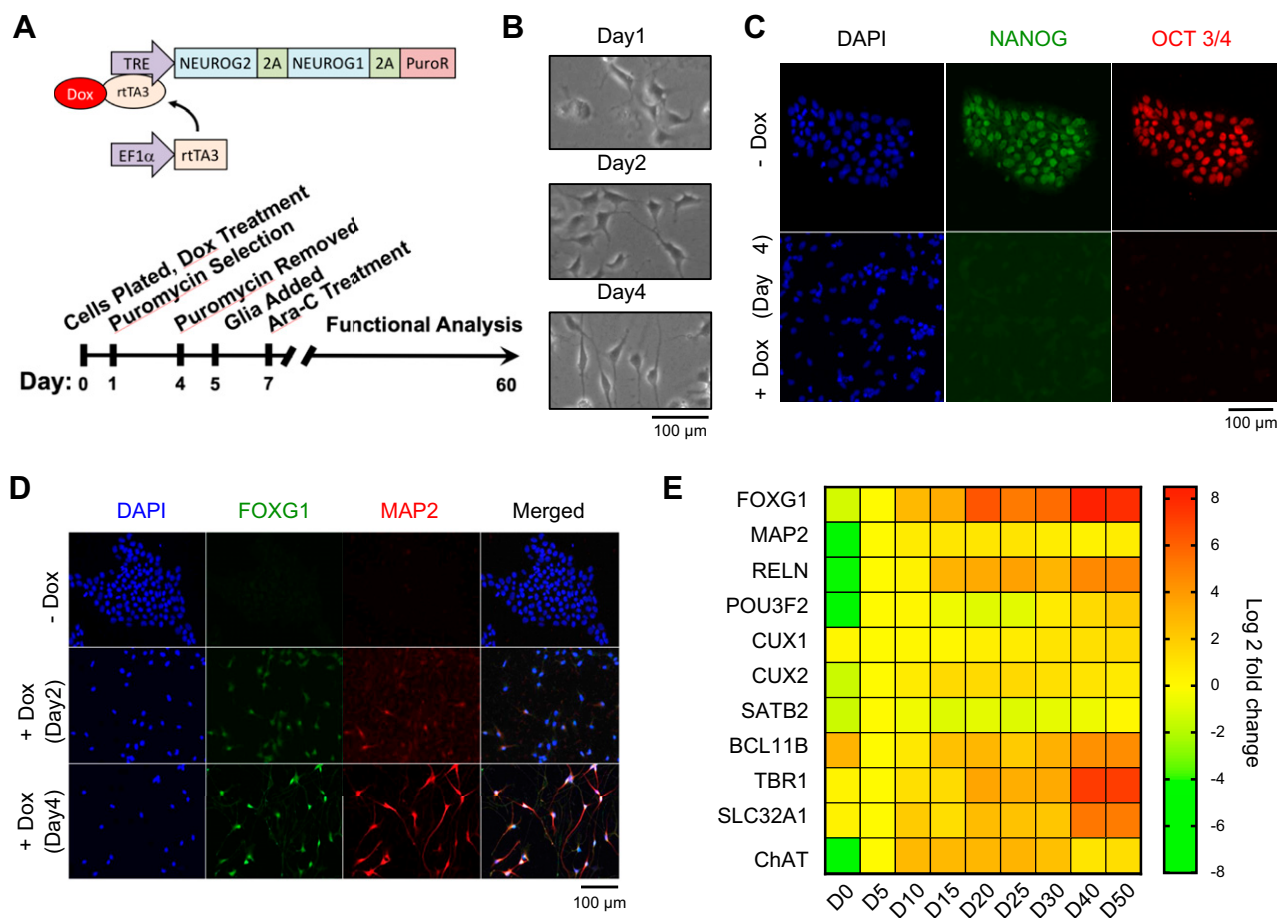
Figure 1. Rapid differentiation of human iNs induced by overexpression of *NEUROG2/1* in hESCs. *A*) Schematic outline of the lentiviral constructs and flow diagram of the differentiation protocol. *B*) Representative phase-contrast images illustrating the changes in cell morphology on d 1, 2, and 4 after doxycyclin (Dox) induction. Scale bar, 100 μm. *C*) Representative immunofluorescence images of hESCs and iN cells immunostained with the stem cell markers Nanog and Oct3/4. One hundred percent of iNs lost staining for both Nanog and Oct3/4 on d 4. Scale bar, 100 μm. *D*) Representative images of hESCs and iN cells immunostained for the neuronal markers FoxG1 and Map2. One hundred percent of iNs were stained for FoxG1 and Map2 on d 4. Scale bar, 100 μm. *E*) Heatmap of gene expression levels of cortical layer markers and neuronal markers in iNs at different days after induction. All expression levels are normalized to those on d 5 (D5). EF1α, elongation factor-1 alpha; PuroR, puromycin resistance gene; rtTA3, reverse tetracycline-controlled transactivator 3; TRE, tetracycline response element.

1 EGTA, 2 Mg-ATP, and 0.2 Na$_3$GTP, with the pH adjusted to 7.4 with KOH. The same internal recording solution was also used for whole-cell recording of the Na-K current voltage clamp in the voltage-clamp configuration. For Ca^{2+} current recordings, the extracellular solution contained (mM) 130 NaCl, 10 BaCl$_2$, and 10 HEPES, and the pH was adjusted to 7.3 with NaOH. To block Na$^+$ currents, all Ca^{2+} current recordings were performed in the presence of 0.5 μM tetrodotoxin (TTX). The internal solution contained (mM) 126 CsCl, 10 EGTA, 1 EDTA, 10 HEPES, and 4 Mg-ATP, and the pH was adjusted to 7.3 with CsOH. The synaptic transmissions were recorded in the whole-cell patch-clamp mode using pipettes filled with CsCl recording solution containing (mM) 120 CsCl, 5 NaCl, 1 MgCl$_2$, 10 HEPES, 10 EGTA, 3 Mg-ATP, 0.3 Na$_4$GTP, and 10 QX-314, with the pH adjusted to 7.2 with NaOH. The excitatory synaptic transmissions were recorded in the whole-cell patch-clamp mode using pipettes filled with K-gluconate recording solution, as previously described. Whole-cell voltage-clamp recordings were made at −70 mV with a MultiClamp 700B Amplifier (Molecular Devices, Sunnyvale, CA, USA) in gap-free mode for at least 5 min for each cell, and access resistance was monitored throughout the recordings. The data were digitized at 10 kHz with a 2-kHz low-pass filter. The liquid junction potential was not corrected and was calculated as 14.8 mV at a recording temperature of 25°C. Data were analyzed offline using Clampfit 10.02 (Molecular Devices) and the MiniAnalysis Program (Synaptosoft, Fort Lee, NJ, USA).

Pharmacological experiments

TTX (1078; Tocris Bioscience, Bristol, United Kingdom) (final concentration of 0.5 μM) was used to isolate miniature synaptic events. NBQX (ab120045; Abcam, Cambridge, MA, USA) (final concentration of 10 μM) was used to remove α-amino-3-hydroxy-5-methyl-4-isoxazolepropionic acid (AMPA) receptor-mediated excitatory synaptic responses. Picrotoxin (1128, PTX; Tocris Bioscience) (final concentration of 20 μM) was used to dissect GABA receptor-mediated inhibitory responses.

Immunocytochemistry

The cells were fixed by incubation with 4% paraformaldehyde and 4% sucrose in PBS at room temperature for 5 min and then washed 3 times with PBS. The fixed cells were permeabilized

with 0.1% Triton X-100/PBS for 5 min, washed 3 times with PBS, and incubated in 3% bovine serum albumin plus 10% normal goat serum in PBS for 1 h to block nonspecific binding. The cells were then incubated overnight with the following primary antibodies at 4°C: mouse anti-NeuN (MAB377, 1:1000; MilliporeSigma), rabbit anti-Nanog (ab80892, 1:500; Abcam), mouse anti-Oct3/4 (sc-5279, 1:500; Santa Cruz Biotechnology, Dallas, TX, USA), rabbit anti-FoxG1 (ab18259, 1:1000; Abcam), mouse anti-Map2 (M1406, 1:500; MilliporeSigma), guinea pig anti-Map2 (188004, 1:1000; SYnaptic SYstems, Goettingen, Germany) and rabbit anti-GABA (A2052, 1:1000; MilliporeSigma). After the cells were washed 3 times with PBS, they were incubated with a secondary goat anti-mouse, Alexa Fluor 555 (A28180, 1:1000; Thermo Fisher Scientific), goat anti-rabbit, Alexa Fluor 555 (A21428, 1:1000; Thermo Fisher Scientific), goat anti-mouse, Alexa Fluor 488 (A32723, 1:1000; Thermo Fisher Scientific), goat anti-rabbit, Alexa Fluor 488 (A11034, 1:1000; Thermo Fisher Scientific), or donkey anti-guinea pig, Alexa 647 (706-605-148, 1:1000; Jackson ImmunoResearch Laboratories, West Grove, PA, USA) antibody. The images were collected using an Axio Cam MRm (Zeiss).

RT-qPCR

No mouse glial cells were added in this set of experiments to avoid amplifying mouse glial genes. At the designated time points for collection, hESCs or iNs were harvested in RLT buffer (Qiagen, Germantown, MD, USA) and stored at −80°C until all time points were collected. Total RNA was extracted using the RNeasy Plus Mini Kit (74134; Qiagen). A total of 90 ng of total RNA was used to generate random-hexamer-primed cDNA from each sample using the Transcriptor First Strand cDNA Synthesis Kit (04896866001; Roche, Basel, Switzerland). qPCR was carried out in technical quadruplicate and biologic triplicate for each time point. Briefly, the samples were processed in 384-well format using a 10-µl total volume with 300 nM forward and reverse primers and FastStart SYBR Green 2X Master Mix (04673484001; Roche) using the following PCR conditions: 10 min at 95°C, followed by 45 cycles of 15 s at 95°C, 30 s at 60°C, and 30 s at 72°C on a LightCycler 480 System (Roche). Raw C_t values were averaged and normalized to a sample-specific ACTB control, and fold changes in gene expression were calculated using the $\Delta\Delta C_t$ method. The primer sequences are listed in Supplemental Table S1. All primer sets were previously validated using RNA from the third trimester human fetal brain (Clontech Laboratories, Mountain View, CA, USA) and HUES66 cells (data not shown), and results from qPCR analysis that did not yield consistent C_t values above 37 cycles were deemed undetectable in our system. Heatmaps were generated by Prism using the $\log_2$ fold changes of the (RT-qPCR results normalized to the level measured on d 5 after NEUROG2/1 induction.

Generating hESC lines with heterogeneous knockout of SCN2A

hESCs (HUES66) were transiently transfected with EF1a-hSpCas9-T2A-EGFP (48138, pX458; Addgene, Watertown, MA, USA) and U6-sgRNA (52963; Addgene), which targets human SCN2A. Similar to the previously described method (17), 24 h later, the transfected cells were enriched for green fluorescent protein–positive cells by fluorescence-activated cell sorting and replated at a low density to encourage the growth of single-cell-derived colonies. Seven to ten days later, each colony was picked, and genomic DNA was extracted and sequenced to obtain all allele genotypes. The karyotypes of hESC lines carrying LOF in 1 allele were validated by TaqMan CNV probes (4400291 and 4403326; Applied Biosystems, Foster City, CA, USA) and used in

this study. One allele from line 1 contains an 8 bp exonic deletion together with a 1 bp intron deletion, whereas the other allele is wild type (WT)-like with a silent mutation. One allele of line 2 contains a 4 bp exonic deletion, and the other allele is WT. The off-target sequences for both sgRNAs were identified using MIT CRISPR tool (http://crispr.mit.edu). SCN2A mRNA expression levels were analyzed using RT-qPCR, as previously described, with forward 5′-GGTTTTATTGTGAGCCTTAG-3′ and reverse 5′-CTTGAAAACTCGGAGCAGCCG-3′ primers.

Statistical analysis

All data were collected from 3 independent batches of cultures. Box and whisker plots were used to show the median and the 5th to 95th percentiles. Data in other plots were shown as means ± SEM. Statistical analyses were performed as indicated in each result.

RESULTS

Generation of iNs by overexpression of NEUROG2/1 in hESCs

hESCs with constitutive expression of reverse tetracycline-controlled transactivator 3 and inducible expression of NEUROG2/1 were generated using a lentiviral delivery system (Fig. 1; see Materials and Methods for details). On d 0, NEUROG2/1-transduced hESCs were plated on Geltrex-coated plates in the presence of doxycycline. The cells were then selected with puromycin from d 1 to 4 for neurogenin expression. Except for the q experiments, mouse glial cells were added on d 5 to support the growth of iNs. Ara-C was added on d 7 to control the growth of the glial cells (Fig. 1A).

Upon overexpression of NEUROG2/1, the hESCs rapidly changed their colonial morphology to a more scattered pattern (Fig. 1B) and completely lost expression of the pluripotency markers Nanog and Oct3/4 on d 4 (Fig. 1C). This change was concurrent with the complete conversion of hESCs to FoxG1- and Map2-positive cells (Fig. 1D). To gain insight into the types of neurons produced, we analyzed the expression of a series of neuronal markers at different time points during the 2-mo culture (Fig. 1E). Our results showed that the expression of FOXG1 and MAP2 increased dramatically within 5 d after NEUROG2/1 induction and remained at high levels throughout the culture period. Similar to Neurog2- and Neurog2/1-differentiated neurons (8, 10), NEUROG2/1 iNs also expressed several superficial cortical layer markers (RELN, POU3F2, CUX2, and SATB), as well as the cholinergic marker choline acetyltransferase. The expression of deep layer marker TBR1 (18, 19) was found to be insignificant (2.4-fold up-regulated expression on d 10 and 11.9-fold up-regulated expression on d 20 compared to that on d 5). Strikingly, we detected the expression of the GABA vesicular transporter SLC32A1 (also known as VGAT) (20) (4-fold up-regulated expression on d 10, 6-fold up-regulated expression on d 20 and 38-fold up-regulated expression on d 40 compared to that on d 5), which was not reported in either Neurog2 or Neurog2/1 iNs (8, 10). To avoid amplifying genes from glial cells, pure iNs in the absence of glial cell coculture were

used for gene expression measurements. As glial cells are crucial for synaptic development (21), the gene expression measured in pure iNs may not fully reflect the function of iNs cocultured with glial cells, which were used for functional analysis later in this report. However, the gene expression in pure *NEUROG2/1* iNs supported the notion that overexpression of *NEUROG2/1* produced a network of both excitatory and inhibitory neurons, even in the absence of glial cells.

Firing properties of *NEUROG2/1* iNs

To characterize the spontaneous firing activity of *NEUROG2/1* iNs, we performed MEA recording (**Fig. 2***A*) and observed reliable firings from approximately d 14 after induction, with a steady increase in activity until the end of our study on d 60 (Fig. 2*B*, *C*). In comparison, primary mouse neurons in culture have been reported to display spontaneous firing activity within the first 7 d after plating (22). Using patch-clamp recording, we further characterized the spontaneous action potentials recorded from *NEUROG2/1* iNs and found them to have an amplitude of 54 ± 1 mV and a rise time of 1.13 ± 0.05 ms on d 60 (Supplemental Fig. S1). As shown in the raster plot in Fig. 2*D*, in addition to an increased spike rate, *NEUROG2/1* iN

networks developed synchronized firing starting on d 25. We calculated the correlation coefficient for the spikes detected from different electrodes on the same MEA at different developmental stages and found that the correlation coefficient increased significantly with development (Fig. 2*E*), indicating an increase in network synchrony over time and suggesting that stronger network connections occur later in development.

To better understand the excitability of *NEUROG2/1* iNs, we characterized their membrane properties using whole-cell patch-clamp recordings. As shown in **Fig. 3***A*, the resting membrane potential of *NEUROG2/1* iNs steadily hyperpolarized from -35 ± 3 mV on d 5 to -54 ± 1 mV on d 60, suggesting that neuronal maturation occurred during this period. Input resistance analysis showed an increase from d 5 to 15, followed by a decrease from d 15 to 60, whereas the membrane capacitance analysis showed a small reduction from d 5 to 15, followed by an increase from d 15 to 60. Voltage-gated K^+ currents appeared on d 5, remained steady between d 5 and 15, and then dramatically increased over time (Fig. 3*C*, left). Unlike voltage-gated K^+ currents, voltage-gated Na^+ currents were hardly detectable on d 5. On d 15, Na^+ currents (0.3 ± 0.1 nA) were present, coinciding with the earliest time point of spontaneous firing activity recorded by MEA (Fig. 2*C*). A dramatic increase in the voltage-gated Na^+ current
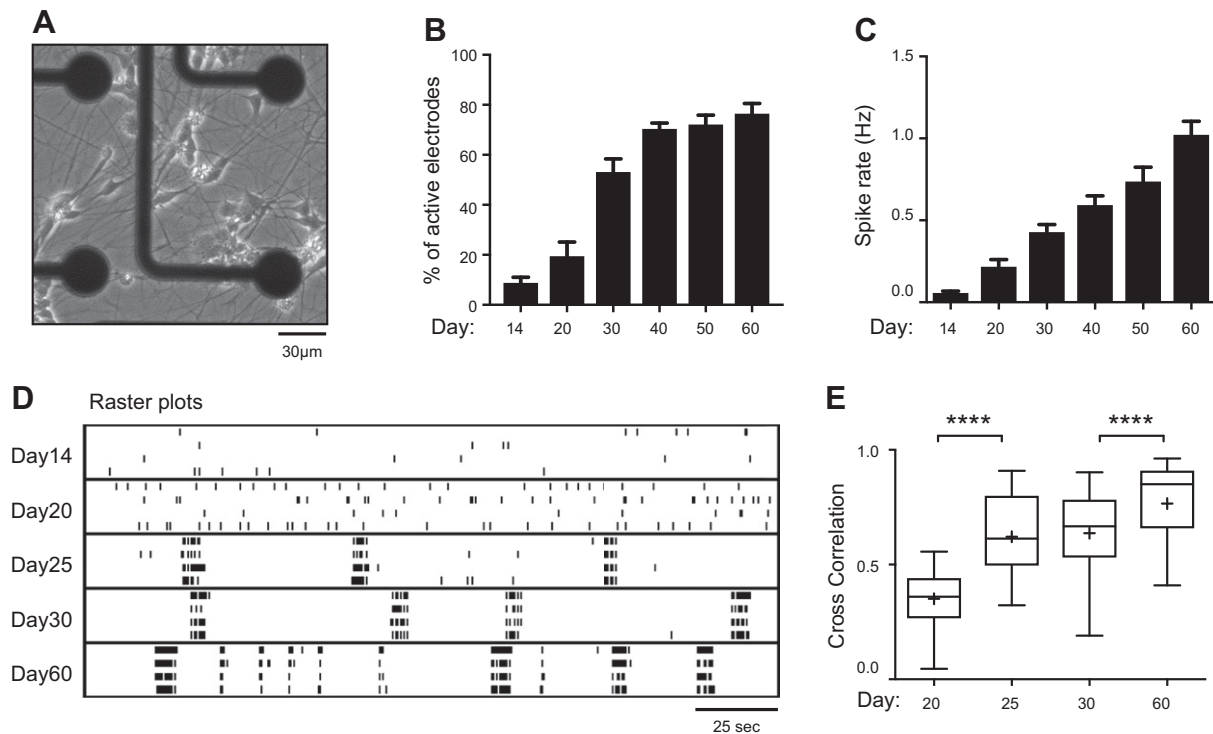
Figure 2. Characterization of the firing activity of iN networks during development. *A*) Phase-contrast image of *NEUROG2/1* iNs on an MEA on d 14. Scale bar, 30 µm. *B*) Quantification of the percentage of active electrodes from iN networks at different time points during development. Data were collected from 9 MEAs. $P < 0.0001$, $F_{(5, 48)} = 50.2$, 1-way ANOVA. *C*) Quantification of the mean spike rate from iN networks at different time points during development. Data were collected from 9 MEAs. $P < 0.0001$, $F_{(5, 766)} = 17.82$, 1-way ANOVA. *D*) Representative raster plots show the spontaneous firing activities recorded from iN networks during development. *E*) Cross correlation analysis of the synchrony of spontaneous firing activities from iN networks on d 20, 25, 30, and 60 after induction. Data were collected from 9 MEAs. Box and whisker plots are used to show the median and the 5th to 95th percentiles. Plus sign indicates the means; 1-way ANOVA, $F_{(3, 3966)} = 385.7$, $P < 0.0001$. ****$P < 0.0001$ Tukey's multiple comparisons test.
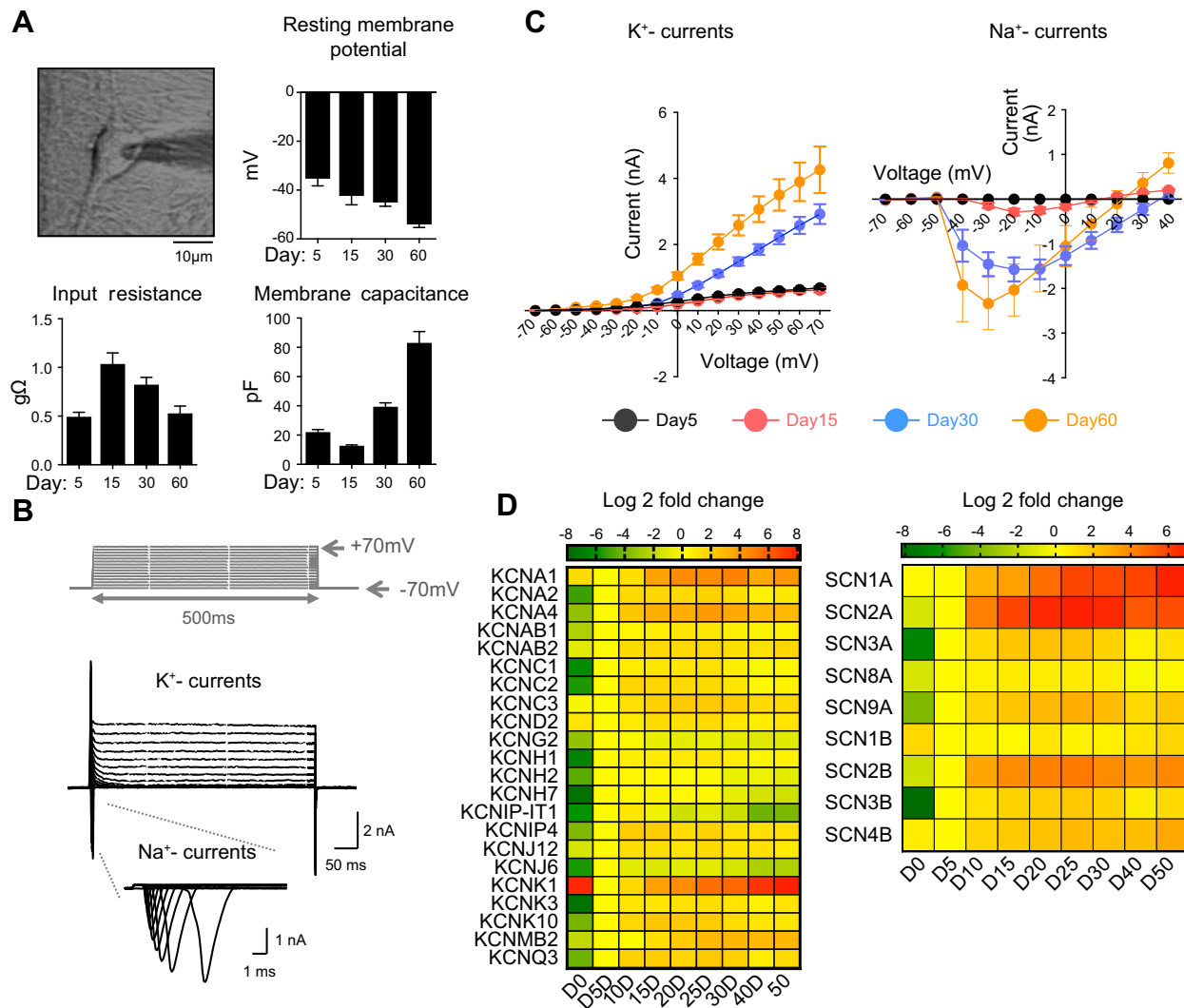
Figure 3. Membrane properties of *NEUROG2/1* iNs. *A*) Phase-contrast image of a *NEUROG2/1* iN during patch-clamp recording (upper left); resting membrane potential (RMP, upper right), input resistance (IR, lower left), and membrane capacitance (MC, lower left) measured by whole-cell patch-clamp recording for iNs on d 5, 15, 30, and 60 after induction. Scale bar, 10 µm. Data were collected from iNs on d 5 ($n = 12$), 15 ($n = 10$), 30 ($n = 27$), and 60 ($n = 33$). $F_{(3,74)} = 17.61$, $P < 0.0001$, 1-way ANOVA for RMP; $F_{(3,36)} = 9.37$, $P < 0.0001$, 1-way ANOVA for IR; $F_{(3,61)} = 67.95$, $P < 0.0001$, 1-way ANOVA for MC. *B*) Representative traces of whole-cell voltage-gated K^+ and Na^+ currents recorded from iNs. Current traces were elicited by depolarizing voltage steps from -70 to $+70$ mV for 500 ms from a holding potential of -70 mV. *C*) Quantification of current/voltage (*I/V*) relationships of K^+ (left) and Na^+ (right) currents from iNs at different time points during development. The K^+ currents were recorded on d 5 ($n = 12$), 15 ($n = 20$), 30 ($n = 20$), and 60 ($n = 13$). The Na^+ currents were recorded on d 5 ($n = 10$), 15 ($n = 16$), 30 ($n = 16$), and 60 ($n = 6$). *D*) Heatmap of the expression levels of genes encoding voltage-gated potassium (left) and sodium (right) channels in iNs during development. All expression levels are normalized to those on d 5 (D5).

(1.6 ± 0.3 nA) was observed on d 30 and was maintained at a similar level until d 60 (Fig. 3*C*, right). As voltage-gated Na^+ and K^+ currents play key roles in neuronal excitability, these observations suggest that *NEUROG2/1* iNs undergo dynamic molecular regulation of membrane excitability during development.

To further understand the molecular identity of the ion channels that contribute to the excitability of *NEUROG2/1* iNs, we performed RT-qPCR at different developmental stages using primers targeting different voltage-gated K^+ and Na^+ channels expressed in the brain (Fig. 3*D*). With the exception of *KCND2* and *KCNK1*, we found that the expression of most neuronal voltage-gated K^+ channel genes peaked between 5 and 15 d after *NEUROG2/1* induction

and remained at elevated levels (Fig. 3*D*, left). Similarly, the expression of most voltage-gated Na^+ channel genes was induced on d 5 (*SCN2A*, *SCN3A*, *SCN8A*, *SCN9A*, *SCN2B*, and *SCN3B*) or d 10 (*SCN1A* and *SCN4B*) and remained elevated throughout the culture period (Fig. 3*D*, right). The time course for gene expression of K^+ channels was largely consistent with their functional conductance, as measured by patch-clamp recordings; however, there was an apparent delay in detecting functional Na^+ currents (on d 15) after the expression of Na^+ channel genes (on d 5), which might be due to regulatory factors specific to Na^+ channels, including the time required for translation, posttranslational modification, and translocation of functional Na^+ channels to the plasma membrane.

Because voltage-gated Ca^{2+} channels are important in multiple cellular functions and have been implicated in the risk of several psychiatric disorders, we next characterized their properties in *NEUROG2/1* iNs (**Fig. 4**). Unlike voltage-gated K^+ or Na^+ currents, which continued to increase after d 15, the observed Ca^{2+} current plateaued between d 10 and 20 and then decreased (Fig. 4*A, B*). Overall, the timeline for the expression of Ca^{2+} channels is consistent with their functional conductance (Fig. 4*C*).

AMPA-excitatory postsynaptic currents dominate synaptic transmissions in *NEUROG2/1* iN networks

To investigate synaptic transmission in *NEUROG2/1* iN networks, we performed whole-cell patch-clamp recordings. Because MEA studies indicated that the spontaneous firing activity of *NEUROG2/1* iNs continued to increase during the 2-mo culture (Fig. 2*C*), we started to evaluate the synaptic events of iNs on d 60 (**Fig. 5*A***, black trace). We applied 0.5 µM TTX to isolate miniature synaptic transmission. In 2 of 12 iNs recorded, 2 types of synaptic events, with either fast rise and decay kinetics (type 1) or slow rise and decay kinetics (type 2), were isolated upon TTX treatment (Fig. 5*A*, red traces). Type 1 events were blocked by the AMPA receptor antagonist NBQX1 (10 µM) (Fig. 5*A*, blue traces), whereas type 2 events were blocked by the GABA receptor antagonist PTX (20 µM) (Fig. 5*A*, gray trace). In the other 10 iNs recorded in the presence of TTX, only type 1 synaptic events were present, which were blocked by NBQX. Quantification of type 1 and type 2 events showed similar peak amplitudes, with type 1 events displaying significantly faster rise and decay kinetics than type 2 events (Fig. 5*B–D*). Taken together, our data suggest that type 1 events represent AMPA receptor-mediated excitatory postsynaptic currents (EPSCs) and that type 2 events represent GABA receptor-mediated inhibitory postsynaptic currents (IPSCs).

Given our finding that EPSCs dominated the synaptic transmissions in the iN networks on d 60, we next focused on characterizing the EPSCs during development. As shown in **Fig. 6*A–C***, EPSCs were detectable on d 21. Although no obvious changes were observed in the average peak amplitude for the spontaneous EPSCs (sEPSCs) over time, the frequency for sEPSCs significantly increased from 0.15 ± 0.02 Hz on d 21 to 25.5 ± 2.01 Hz on d 60. In the presence of TTX treatment, we measured miniature excitatory postsynaptic currents (mEPSCs) from d 21 to 60. As shown in Fig. 6*D–F*, mEPSCs had small yet significant reductions in peak amplitude from d 30 to 60, whereas their frequency dramatically increased over time (from 0.12 ± 0.03 Hz on d 21 to 2.7 ± 0.52 Hz on d 60), suggesting that increased synapse formation is the dominant functional change between d 21 and 60.

GABAergic iNs play a significant role in regulating spontaneous network firing activity

As we identified the expression of GABAergic markers in RT-qPCR analysis (Fig. 1*E*) and IPSCs in patch-clamp recordings (Fig. 5*A*), we hypothesized that functional GABAergic neurons were present in the *NEUROG2/1* iN network. We performed ICC with an anti-GABA antibody and found GABA-positive cells in the iN networks (**Fig. 7*A***). The percentage of GABA-positive iNs on d 30 was analyzed and found to be $2.3\% \pm 0.3\%$. To exclude contamination with GABAergic neurons from cocultured mouse glial cells, we cultured iNs alone and confirmed that immunostaining of GABA was also present in pure iN cultures (Supplemental Fig. S2). To understand the developmental profile of the GABAergic iNs, we performed
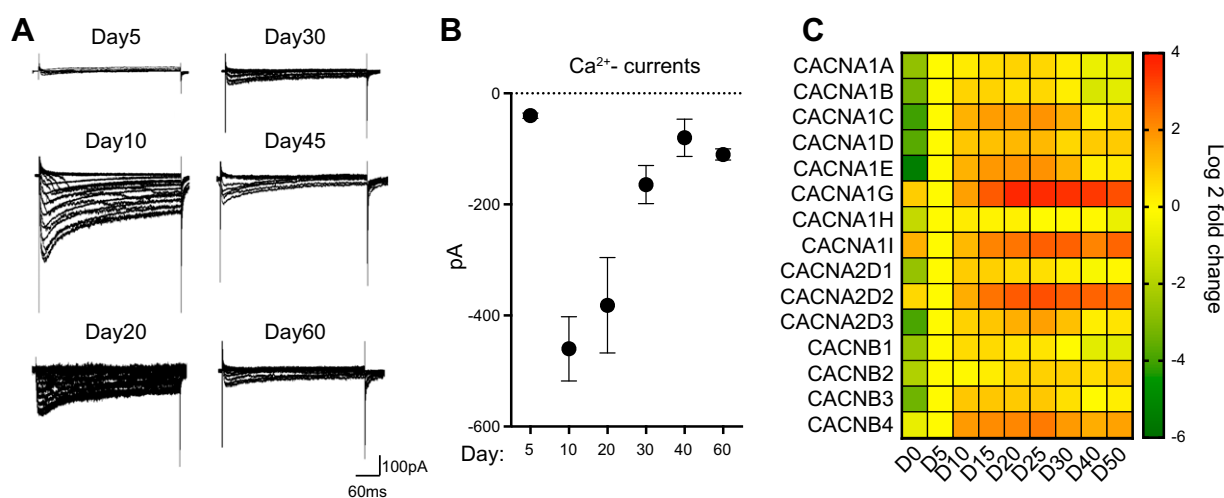
Figure 4. Characterization of voltage-gated calcium channels in *NEUROG2/1* iNs. *A*) Representative traces of whole-cell Ca^{2+} currents recorded in *NEUROG2/* iNs at different time points during development. Current traces were elicited by depolarizing voltage steps from −80 to +20 mV for 200 ms at a holding potential of −100 mV. *B*) Quantification of Ca^{2+} currents. The Ca^{2+} currents were recorded on d 5 (*n* = 6), 10 (*n* = 5), 20 (*n* = 6), 30 (*n* = 7), 45 (*n* = 4), and 60 (*n* = 3). *C*) Heatmap of expression levels of genes encoding voltage-gated calcium channels in iNs during development. All expression levels are normalized to those on d 5 (D5).
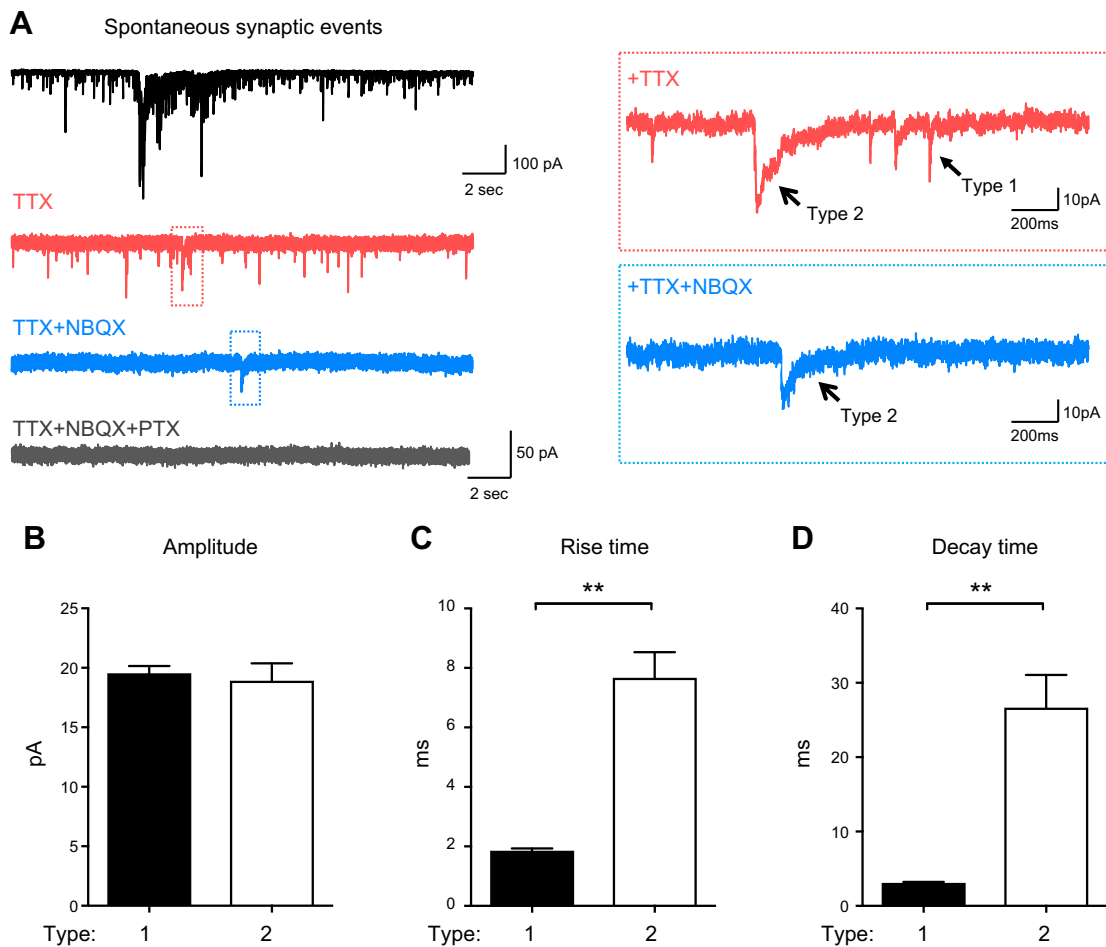
Figure 5. Characterization of the synaptic activities of *NEUROG2/1* iN networks. *A*) Representative traces of spontaneous (black trace) and pharmacologically isolated synaptic events (red, blue, and gray traces) recorded from iN networks by whole-cell patch-clamp recording on d 60. Two types of miniature synaptic events were observed after TTX (0.5 μM) treatment (red traces). Type 1 miniature synaptic events were depleted upon NBQX (10 μM) treatment (blue traces). Type 2 miniature synaptic events were depleted by additional PTX treatment (20 μM) (gray trace). *B–D*) Quantification of the amplitude (*B*), rise time (*C*), and decay time (*D*) for the type 1 and type 2 synaptic events. The analysis of type 1 and type 2 events included recordings of 12 and 2 iNs, respectively. **$P < 0.01$ (unpaired Student's *t* test).

RT-qPCR to evaluate the expression of GABAergic markers in pure iN cultures at different time points (Fig. 7*B*). Similar to the expression of the GABA vesicular transporters *SLC32A1*, *GAD1*, and *GAD*2, the proteins that catalyze the conversion of glutamate to GABA also showed a modest but steady increase in expression with development (2.1- and 1.8-fold increased expression, respectively, on d 15 and 6.8- and 6.2-fold increased expression, respectively, on d 40 compared to that on d 5). The expression of *LHX5*, which has been found in dorsal spinal cord interneurons and in Cajal-Retzius cells that play important roles in the lamination of the mammalian cortex (23, 24), increased 19-fold on d 5 and then remained at the same level throughout the culture. The expression of *LHX6*, which has been reported to be involved in the migration and specification of cortical interneurons (25), was found to be insignificant (10-fold on d 25 compared to that on d 5). The expression of the transcription factors *DLX2* and *DLX5* in GABAergic neurons (26) showed 13- and 4-fold increases on d 20, respectively, and 184- and 7.2-fold increases on d 40, respectively, compared to that on d 5.

These data collectively showed that multiple molecular inhibitory neuronal markers are present in *NEUROG1/2* iNs. To evaluate the functional role of GABAergic iNs in the network, we treated *NEUROG2/1* iN networks with the GABA receptor antagonist PTX (20 μM) on d 60 and found that the network firing rate significantly increased upon PTX treatment (Fig. 7*C*), suggesting that inhibitory synaptic transmission played a significant role in regulating the spontaneous firing of *NEUROG2/1* iN networks during the later developmental stage.

Heterozygous knockout of *SCN2A* led to hypoactive *NEUROG2/1* iN networks

To explore the application of *NEUROG2/1* iNs, we studied the functional impact of disrupting *SCN2A* on the *NEUROG2/1* iN network. *SCN2A* encodes the voltage-gated sodium channel α subunit Na$_v$1.2, and its heterozygous LOF has been associated with autism spectrum disorders (ASD) and other neurologic disorders (12–15).
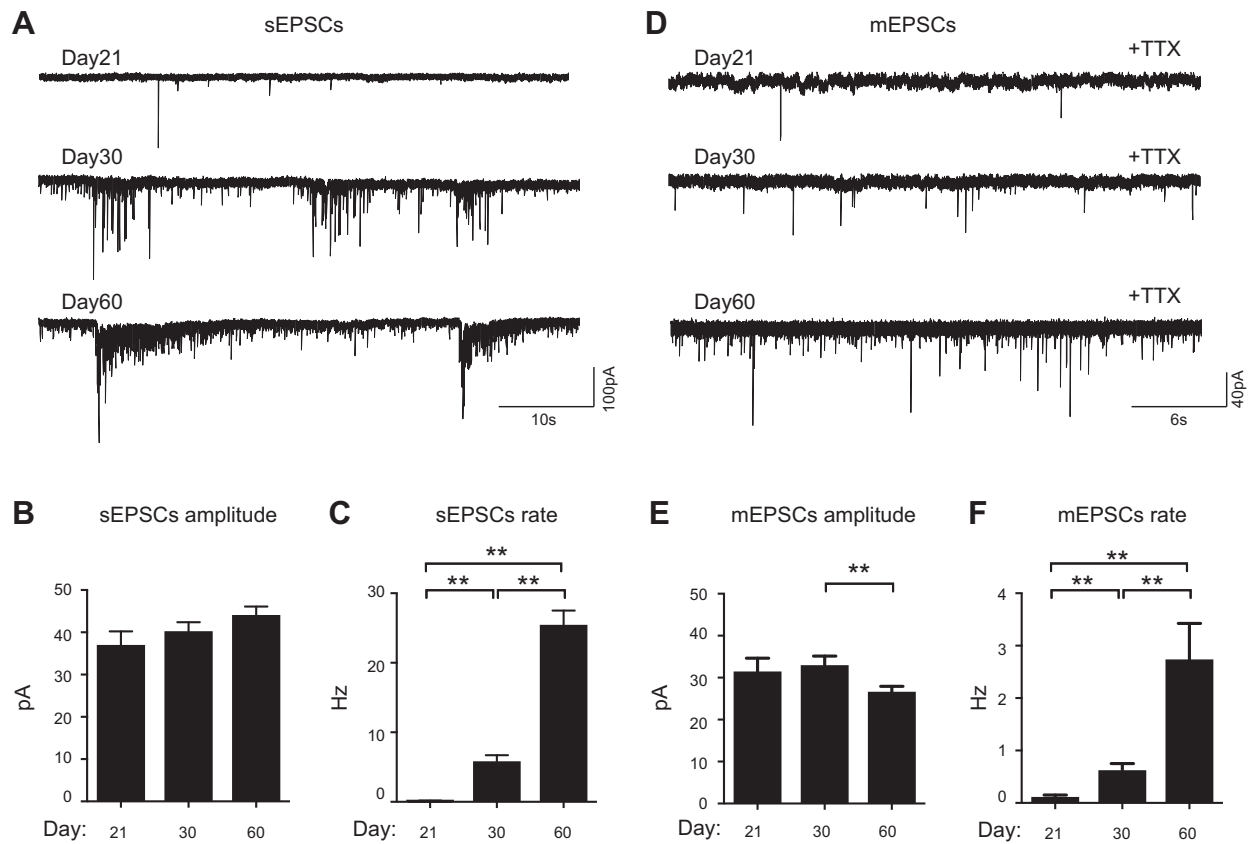
Figure 6. Developmental changes in the excitatory synaptic transmission of iN networks. *A*) Representative traces of sEPSCs recorded from iNs on d 21, 30, and 60. *B, C*) Quantification of the amplitude (*B*) and frequency (*C*) of the sEPSCs during development. *D*) Representative traces of mEPSCs recorded from iN cells on d 21, 30, and 60 after induction. *E, F*) Quantification of the amplitude (*E*) and frequency (*F*) of the mEPSCs during development. The analyses of sEPSCs included recordings of 16, 27, and 27 iNs on d 21, 30, and 60, respectively; analyses of mEPSCs included recordings of 5, 12, and 22 iNs on d 21, 30, and 60, respectively. **$P < 0.01$ (unpaired Student's *t* test).

As *SCN2A* is expressed in *NEUROG2/1* iNs (Fig. 3*D*), we set out to model *SCN2A* LOF using *NEUROG2/1* iNs. As shown in **Fig. 8*A***, 2 hESC lines with heterozygous knockout of *SCN2A* (*SCN2A*$^{+/-}$) were produced with CRISPR/Cas9-mediated genome engineering (16). Sanger sequencing indicated that both lines contained 1 WT-like allele and 1 edited allele that was predicted to produce premature stop codons (Fig. 8*B*) (premature stop codon at aa 872 for line 1 and aa 1077 for line 2; RefSeq NM_021007.2). The raw Sanger sequencing reads for both lines around the engineered locations are shown in Supplemental Fig. S3. To evaluate the potential off-target effects, we identified the top 5 predicted off-target sequences for both sgRNAs and Sanger sequencing verified that those sites were free of mutations (Supplemental Fig. S4). Using the same method described in Fig. 1*A*, we transduced *SCN2A*$^{+/-}$ hESCs with *NEUROG2/1* and differentiated them into neurons. RT-qPCR studies revealed an ~50% reduction in the *SCN2A* mRNA level for both *SCN2A*$^{+/-}$ iNs, validating the LOF of *SCN2A* in both lines (Fig. 8*C*). Subsequently, we monitored the spontaneous firing activities in *SCN2A*$^{+/-}$ iN networks during development and found that the spike rates of *SCN2A*$^{+/-}$ networks were reduced compared to those of WT networks throughout development (Fig. 8*D*). These

data, for the first time, demonstrated significant functional deficits in neurons with LOF of *SCN2A* on a human genomic background. After PTX treatment on d 60, the spike rate of *SCN2A*$^{+/-}$ iN networks increased ~2-fold, similar to the observation in WT iN networks (Fig. 8*F*). Taken together, our data suggested that heterozygous knock out of *SCN2A* led to a significant reduction in spontaneous network firing activity but did not impair the functional role of inhibitory synaptic transmission in the network.

DISCUSSION

Previous studies have shown that overexpression of *Neurog2* or *Neurog2/1* in hESCs and hiPSCs can rapidly and efficiently produce excitatory neurons (8, 10, 11, 27, 28). Here, we established *NEUROG2/1* iNs and monitored their molecular, cellular, and electrophysiological properties over 60 d after induction. We found that overexpression of *NEUROG1* and *NEUROG2* in hESCs induced a network with both glutamatergic excitatory and GABAergic inhibitory neurons.

Although only a small portion of *NEUROG2/1* iNs were found to be GABAergic (2.3 ± 0.3% on d 30), MEA
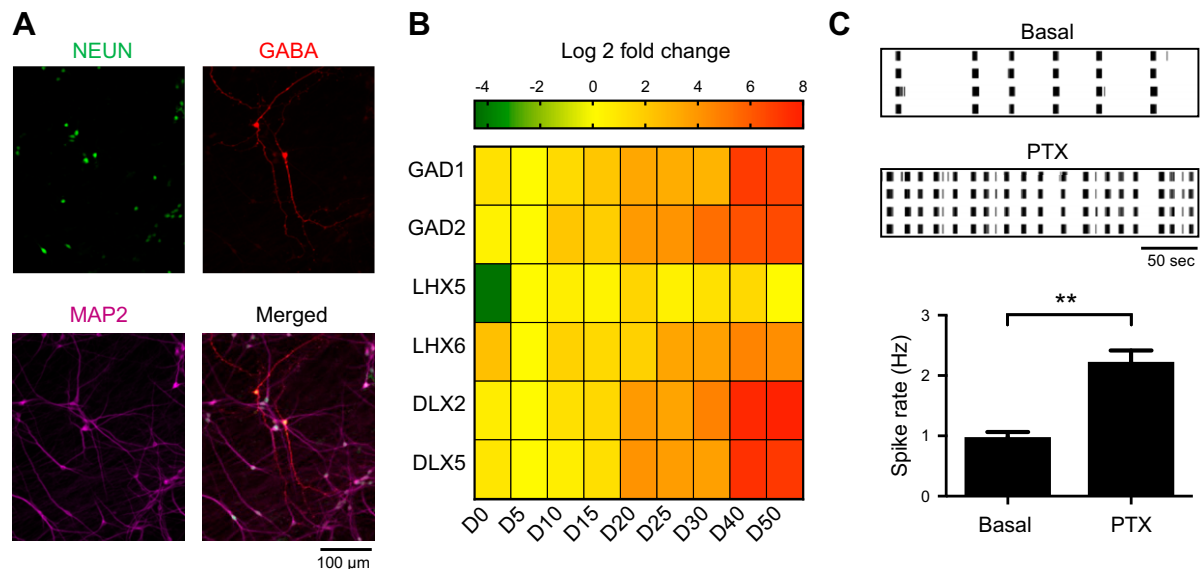
Figure 7. GABAergic neurons developed in the *NEUROG2/1* iN networks. *A*) Representative iNs immunostained for NeuN (green), GABA (red), and Map2 (purple) on d 30. Scale bar, 100 μm. *B*) Heatmap of the expression levels of genes encoding inhibitory molecular markers at different days after induction. All expression levels are normalized to those on d 5 (D5). *C*) Representative raster plots (top) and analysis of the spike rate (bottom) of iN networks recorded by MEA on d 60 before and after PTX (20 μM) treatment. Data were collected from 6 MEAs. **$P < 0.01$ (unpaired Student's *t* test).

recordings revealed a 2-fold increase in the network spiking rate in response to PTX treatment to block inhibitory transmission (Fig. 7*C*), demonstrating the significant functional role of inhibitory neurons in the *NEUROG2/1* iN network. GABAergic cells were not previously reported to develop from *Neurog2* (8) or *Neurog2/1* iNs (10, 11). Last year, a report showed that forced expression of *Neurog2* in the presence of *Dlx2* could produce a network with glutamatergic and GABAergic neurons, whereas *Neurog2* in combination with any other transcription factors, such as *Lhx1* and *Pax2*, induced only glutamatergic excitatory neurons (25). Our data indicated that *NEUROG2* in combination with *NEUROG1* produced a neuronal network with both excitatory and inhibitory neurons (Figs. 5*A* and 7). Because many conditions were changed in our experiments compared to previous experiments, such as the cells used for differentiation, the source of glial cells, and the culture conditions, it is not clear which particular factor/factors triggered the induction of GABAergic cells in our protocol. Among all these variations, having human, not mouse, neurogenins might play an important role because the protein sequences encoded by *NEUROG2/1* and *Neurog2/1* are not identical (Supplemental Fig. S5). *Neurog2*, as a pioneer transcription factor, can open chromatin structures to allow the binding of secondary transcription factors that facilitate the expression of more mature or subtype-specific proteins (29). The difference in protein sequence might allow *NEUROG2* alone or in combination with *NEUROG1* to activate additional transcription factors compared to *Neurog2/1*, which could promote the induction of GABAergic neurons. It will be important to perform more experiments in the future to test this hypothesis, which might result in new strategies to generate exclusively GABAergic neurons.

In this study, we followed *NEUROG2/1* iNs up to 60 d after induction and found that they could be easily maintained in culture. As shown in the MEA and patch-clamp characterizations, spontaneous firing and synaptic transmission became more active with development, showing no plateau (or decrease) throughout the 60-d period (Figs. 2 and 6). Compared to *Neurog2/1* iNs (11), the *NEUROG2/1* iNs showed some nonsignificant differences in their intrinsic membrane properties (~1.3-fold depolarization of the resting membrane potential, 1.5-fold decrease in input resistance, and 1.6-fold increase in membrane capacitance on approximately d 60). Interestingly, the excitatory synaptic transmissions detected from *NEUROG2/1* iNs were dramatically more active than those reported from *Neurog2/1* iNs (an ~32-fold increase in the sEPSC rate on approximately d 60). The increase in the sEPSC rate suggested that the *NEUROG2/1* iNs developed into a network with much more spontaneous activity. As discussed earlier, different experimental conditions, such as the type of cells used for differentiation (hESCs *vs.* iPSCs), the source of glial cells (mouse *vs.* rat) for coculture, and the culture protocol (plating glial cells after iNs *vs.* plating glial cells before iNs), might cause the observed differences in spontaneous activity.

It is known that the construction of neural circuits in the CNS is a dynamic process involving the formation and elimination of synapses to sharpen the neural circuitry (30, 31). Although the spontaneous firing and synaptic activity of *NEUROG2/1* iNs continued to increase over time, the observed activities never reached a plateau (or decrease) during the 60-d culture period. It is likely that the *NEUROG2/1* iN network still reflects the early developmental stages of neuronal assembly before the synaptic connections are saturated. Nevertheless, given that reliable robust synaptic and firing activities developed in
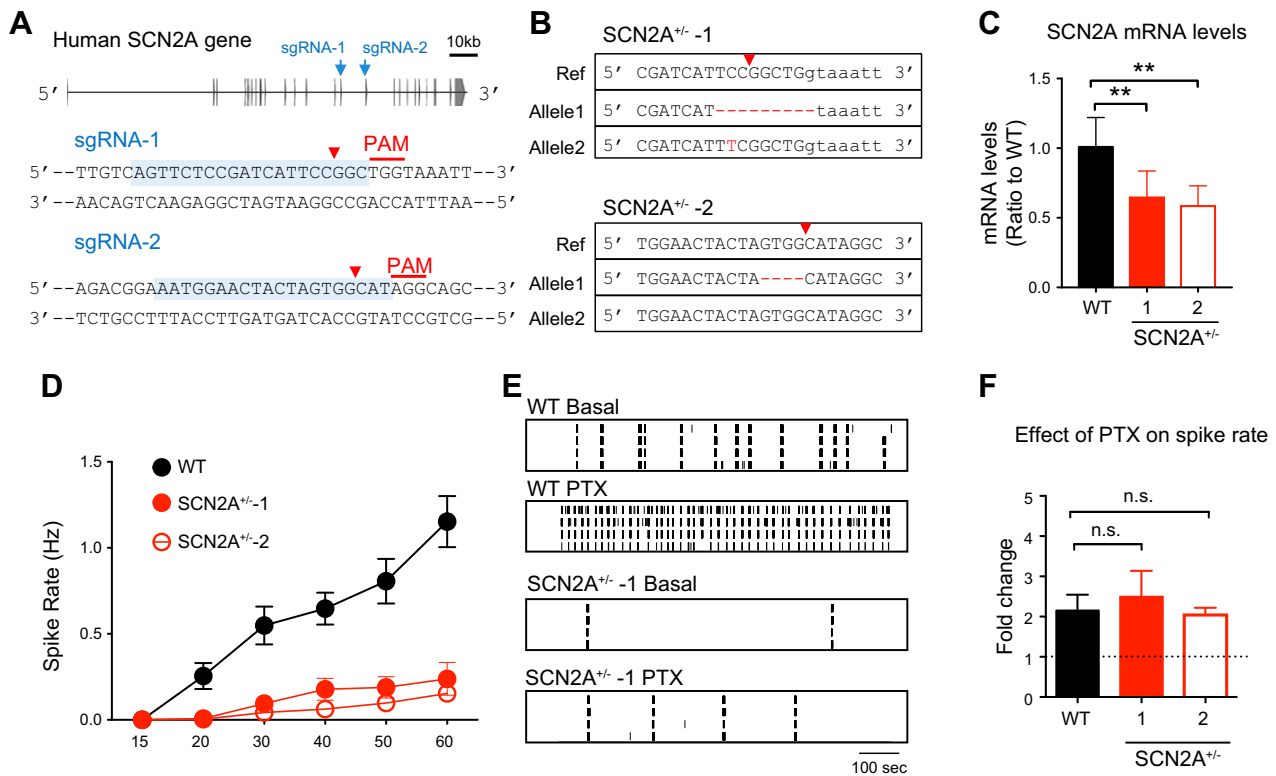
Figure 8. Impaired network firing in $SCN2A^{+/-}$ iN networks. *A*) Schematic illustration of the strategy for establishing $SCN2A^{+/-}$ hESCs using CRISPR/Cas9 genome editing. The locations of sgRNAs targeting the human *SCN2A* gene are indicated by blue arrows (top panel) and highlighted in light blue, with the corresponding protospacer-adjacent motif (PAM) in red (bottom panels). Red arrowheads indicate predicted double-stranded break (DSB) sites. *B*) Sequencing results from 2 monoclonal hESC lines ($SCN2A^{+/-}$-1 and $SCN2A^{+/-}$-2) produced with sgRNA-1 and sgRNA-2, respectively. Red arrowheads indicate predicted DSB sites. Mutant sequences are highlighted in red. Uppercase sequence indicates exons, and lowercase sequence indicates introns. *C*) The mRNA expression levels of *SCN2A* in the 2 $SCN2A^{+/-}$ lines, normalized to the expression of *SCN2A* in WT iNs. *D*) Quantification of the mean spike rate of WT, $SCN2A^{+/-}$-1, and $SCN2A^{+/-}$-2 iN networks at different time points during development. Data were collected from 9 MEAs for each line. *E*) Representative raster plots of network activities of WT and $SCN2A^{+/-}$-1 iN networks recorded by MEA at d 60 in the absence and presence of PTX (20 μM) treatment. *F*) Analysis of the fold change in the spike rate for WT and $SCN2A^{+/-}$ iN networks in response to PTX (20 μM) treatment. Data were collected from 9 MEAs for each line. N,s., not significant. **$P < 0.01$ (unpaired Student's *t* test).

such networks with both excitatory and inhibitory neurons (Figs. 2 and 6), *NEUROG2/1* iNs could be useful for modeling neurodevelopmental disorders.

To demonstrate the utility of *NEUROG2/1* iNs, we engineered hESCs with LOF in 1 allele of *SCN2A* and differentiated them into neurons by overexpressing *NEUROG2/1*. *SCN2A* encodes the voltage-gated sodium channel Na$_v$1.2, which is critical for the generation and propagation of action potentials. Gain-of-function variants in the *SCN2A* gene have been implicated in infantile seizures (12, 32, 33), whereas LOF variants have been implicated in ASDs (13, 34, 35). Homozygous LOF of *SCN2A* is lethal in mice (36), and haploinsufficiency of *SCN2A* produces seizure-like activities (37). A recent study using HEK293 cells expressing WT or ASD-associated mutant *SCN2A* showed that ASD-associated mutations impaired Na$_v$1.2 channel function, and a predicted ASD-associated *SCN2A* mutation led to a reduction in neuronal excitability using computational models (12). Our data showed that heterogeneous knockout of *SCN2A* produced a hypoactive human neuronal network with a drastic reduction in neuronal firing frequency, as revealed by MEA. Such a

cellular phenotype could be used to study the mechanism through which *SCN2A* influences network excitability and may serve as a cellular phenotype applicable to screening compounds for rescuing defects. Our study not only identified a cellular phenotype caused by the LOF of *SCN2A* but also substantiated *NEUROG2/1* iNs as a neuronal model system that may be useful for studying the function of human genes implicated in neurodevelopmental disorders.

Over the past decade, genetic studies have identified a growing list of *de novo* mutations in patients with neurodevelopmental and neuropsychiatric diseases (38–40). A key challenge is the lack of relevant, efficient, and accessible human neuronal models for studying the causative effects of those mutations. Genome engineering combined with stem cell reprogramming enables fast and accurate engineering of hESCs with desired mutations for modeling psychiatric disorders in a human neuronal context. Through in-depth characterization of iN networks with overexpression of *NEUROG2/1*, we found that this model system contained both excitatory and inhibitory neurons and exhibited robust spontaneous network activity within

1 mo. In combination with high-throughput assays, such as MEA, *NEUROG2/1* human iNs could be valuable for many applications, such as neurophenotyping the *de novo* mutations identified from genetic studies of disease and modeling neurodevelopmental diseases with the appropriate human genetic background. **FJ**

AUTHOR CONTRIBUTIONS

C. Lu, X. Shi, and J. Q. Pan designed the study; C. Lu conducted electrophysiology experiments other than Ca^{2+} current recordings; D. Baez-Nieto conducted Ca^{2+} current recordings; A. Allen conducted RT-qPCR experiments; C. Lu and A. Nikish conducted ICC; N. E. Sanjana generated the *NEUROG2/1* lentivirus; X. Shi and N. E. Sanjana initiated the project on iNs and generated *SCN2A*$^{+/−}$ hESCs; C. Lu, X. Shi, and J. Q. Pan drafted the manuscript; J. Q. Pan supervised the study; and all authors contributed to the editing of the manuscript.

REFERENCES

1. Hafezparast, M., Ahmad-Annuar, A., Wood, N. W., Tabrizi, S. J., and Fisher, E. M. C. (2002) Mouse models for neurological disease. *Lancet Neurol.* **1**, 215–224
2. Chesselet, M.-F., and Carmichael, S. T. (2012) Animal models of neurological disorders. *Neurotherapeutics* **9**, 241–244
3. Avior, Y., Sagi, I., and Benvenisty, N. (2016) Pluripotent stem cells in disease modelling and drug discovery. *Nat. Rev. Mol. Cell Biol.* **17**, 170–182
4. Hibaoui, Y., and Feki, A. (2012) Human pluripotent stem cells: applications and challenges in neurological diseases. *Front. Physiol.* **3**, 267
5. Thomson, J. A., Itskovitz-Eldor, J., Shapiro, S. S., Waknitz, M. A., Swiergiel, J. J., Marshall, V. S., and Jones, J. M. (1998) Embryonic stem cell lines derived from human blastocysts. *Science* **282**, 1145–1147
6. Takahashi, K., Tanabe, K., Ohnuki, M., Narita, M., Ichisaka, T., Tomoda, K., and Yamanaka, S. (2007) Induction of pluripotent stem cells from adult human fibroblasts by defined factors. *Cell* **131**, 861–872
7. Nakagawa, M., Koyanagi, M., Tanabe, K., Takahashi, K., Ichisaka, T., Aoi, T., Okita, K., Mochiduki, Y., Takizawa, N., and Yamanaka, S. (2008) Generation of induced pluripotent stem cells without Myc from mouse and human fibroblasts. *Nat. Biotechnol.* **26**, 101–106
8. Zhang, Y., Pak, C., Han, Y., Ahlenius, H., Zhang, Z., Chanda, S., Marro, S., Patzke, C., Acuna, C., Covy, J., Xu, W., Yang, N., Danko, T., Chen, L., Wernig, M., and Südhof, T. C. (2013) Rapid single-step induction of functional neurons from human pluripotent stem cells. *Neuron* **78**, 785–798
9. Gascón, S., Masserdotti, G., Russo, G. L., and Götz, M. (2017) Direct neuronal reprogramming: achievements, hurdles, and new roads to success. *Cell Stem Cell* **21**, 18–34
10. Busskamp, V., Lewis, N. E., Guye, P., Ng, A. H. M., Shipman, S. L., Byrne, S. M., Sanjana, N. E., Murn, J., Li, Y., Li, S., Stadler, M., Weiss, R., and Church, G. M. (2014) Rapid neurogenesis through transcriptional activation in human stem cells. *Mol. Syst. Biol.* **10**, 760
11. Lam, R. S., Töpfer, F. M., Wood, P. G., Busskamp, V., and Bamberg, E. (2017) Functional maturation of human stem cell-derived neurons in long-term cultures. *PLoS One* **12**, e0169506
12. Ben-Shalom, R., Keeshen, C. M., Berrios, K. N., An, J. Y., Sanders, S. J., and Bender, K. J. (2017) Opposing effects on Na$_V$1.2 function underlie differences between SCN2A variants observed in individuals with autism spectrum disorder or infantile seizures. *Biol. Psychiatry* **82**, 224–232
13. Sanders, S. J., He, X., Willsey, A. J., Ercan-Sencicek, A. G., Samocha, K. E., Cicek, A. E., Murtha, M. T., Bal, V. H., Bishop, S. L., Dong, S., Goldberg, A. P., Jinlu, C., Keaney III, J. F., Klei, L., Mandell, J. D., Moreno-De-Luca, D., Poultney, C. S., Robinson, E. B., Smith, L., Solli-Nowlan, T., Su, M. Y., Teran, N. A., Walker, M. F., Werling, D. M., Beaudet, A. L., Cantor, R. M., Fombonne, E., Geschwind, D. H., Grice, D. E., Lord, C., Lowe, J. K., Mane, S. M., Martin, D. M., Morrow, E. M., Talkowski, M. E., Sutcliffe, J. S., Walsh, C. A., and Yu, T. W.; Autism Sequencing Consortium. (2015) Insights into autism spectrum disorder genomic architecture and biology from 71 risk loci. *Neuron* **87**, 1215–1233
14. Deciphering developmental disorders study. (2015) Large-scale discovery of novel genetic causes of developmental disorders. *Nature* **519**, 223–228
15. Howell, K. B., McMahon, J. M., Carvill, G. L., Tambunan, D., Mackay, M. T., Rodriguez-Casero, V., Webster, R., Clark, D., Freeman, J. L., Calvert, S., Olson, H. E., Mandelstam, S., Poduri, A., Mefford, H. C., Harvey, A. S., and Scheffer, I. E. (2015) SCN2A encephalopathy: a major cause of epilepsy of infancy with migrating focal seizures. *Neurology* **85**, 958–966
16. Cong, L., Ran, F. A., Cox, D., Lin, S., Barretto, R., Habib, N., Hsu, P. D., Wu, X., Jiang, W., Marraffini, L. A., and Zhang, F. (2013) Multiplex genome engineering using CRISPR/Cas systems. *Science* **339**, 819–823
17. Peters, D. T., Cowan, C. A., and Musunuru, K. (2008) Genome editing in human pluripotent stem cells. In *StemBook*, Harvard Stem Cell Institute, Cambridge, MA, USA
18. Molyneaux, B. J., Arlotta, P., Menezes, J. R. L., and Macklis, J. D. (2007) Neuronal subtype specification in the cerebral cortex. *Nat. Rev. Neurosci.* **8**, 427–437
19. Zhang, J., and Jiao, J. (2015) Molecular biomarkers for embryonic and adult neural stem cell and neurogenesis. *BioMed Res. Int.* **2015**, 727542
20. McIntire, S. L., Reimer, R. J., Schuske, K., Edwards, R. H., and Jorgensen, E. M. (1997) Identification and characterization of the vesicular GABA transporter. *Nature* **389**, 870–876
21. Neniskyte, U., and Gross, C. T. (2017) Errant gardeners: glial-cell-dependent synaptic pruning and neurodevelopmental disorders. *Nat. Rev. Neurosci.* **18**, 658–670
22. Lu, C., Chen, Q., Zhou, T., Bozic, D., Fu, Z., Pan, J. Q., and Feng, G. (2016) Micro-electrode array recordings reveal reductions in both excitation and inhibition in cultured cortical neuron networks lacking Shank3. *Mol. Psychiatry* **21**, 159–168
23. Pillai, A., Mansouri, A., Behringer, R., Westphal, H., and Goulding, M. (2007) Lhx1 and Lhx5 maintain the inhibitory-neurotransmitter status of interneurons in the dorsal spinal cord. *Development* **134**, 357–366
24. Miquelajáuregui, A., Varela-Echavarría, A., Ceci, M. L., García-Moreno, F., Ricaño, I., Hoang, K., Frade-Pérez, D., Portera-Cailliau, C., Tamariz, E., De Carlos, J. A., Westphal, H., and Zhao, Y. (2010) LIM-homeobox gene Lhx5 is required for normal development of Cajal-Retzius cells. *J. Neurosci.* **30**, 10551–10562
25. Liodis, P., Denaxa, M., Grigoriou, M., Akufo-Addo, C., Yanagawa, Y., and Pachnis, V. (2007) Lhx6 activity is required for the normal migration and specification of cortical interneuron subtypes. *J. Neurosci.* **27**, 3078–3089
26. Yang, N., Chanda, S., Marro, S., Ng, Y.-H., Janas, J. A., Haag, D., Ang, C. E., Tang, Y., Flores, Q., Mall, M., Wapinski, O., Li, M., Ahlenius, H., Rubenstein, J. L., Chang, H. Y., Buylla, A. A., Südhof, T. C., and Wernig, M. (2017) Generation of pure GABAergic neurons by transcription factor programming. *Nat. Methods* **14**, 621–628
27. Frega, M., van Gestel, S. H. C., Linda, K., van der Raadt, J., Keller, J., Van Rhijn, J.-R., Schubert, D., Albers, C. A., and Nadif Kasri, N. (2017) Rapid neuronal differentiation of induced pluripotent stem cells for measuring network activity on micro-electrode arrays. *J. Vis. Exp.* **119**, e54900
28. Ho, S.-M., Hartley, B. J., Tcw, J., Beaumont, M., Stafford, K., Slesinger, P. A., and Brennand, K. J. (2016) Rapid Ngn2-induction of excitatory

neurons from hiPSC-derived neural progenitor cells. *Methods* **101**, 113–124

29. Mertens, J., Marchetto, M. C., Bardy, C., and Gage, F. H. (2016) Evaluating cell reprogramming, differentiation and conversion technologies in neuroscience. *Nat. Rev. Neurosci.* **17**, 424–437

30. Lichtman, J. W., and Colman, H. (2000) Synapse elimination and indelible memory. *Neuron* **25**, 269–278

31. Hua, J. Y., and Smith, S. J. (2004) Neural activity and the dynamics of central nervous system development. *Nat. Neurosci.* **7**, 327–332

32. Xu, R., Thomas, E. A., Jenkins, M., Gazina, E. V., Chiu, C., Heron, S. E., Mulley, J. C., Scheffer, I. E., Berkovic, S. F., and Petrou, S. (2007) A childhood epilepsy mutation reveals a role for developmentally regulated splicing of a sodium channel. *Mol. Cell. Neurosci.* **35**, 292–301

33. Schwarz, N., Hahn, A., Bast, T., Müller, S., Löffler, H., Maljevic, S., Gaily, E., Prehl, I., Biskup, S., Joensuu, T., Lehesjoki, A.-E., Neubauer, B. A., Lerche, H., and Hedrich, U. B. S. (2016) Mutations in the sodium channel gene SCN2A cause neonatal epilepsy with late-onset episodic ataxia. *J. Neurol.* **263**, 334–343

34. Iossifov, I., O'Roak, B. J., Sanders, S. J., Ronemus, M., Krumm, N., Levy, D., Stessman, H. A., Witherspoon, K. T., Vives, L., Patterson, K. E., Smith, J. D., Paeper, B., Nickerson, D. A., Dea, J., Dong, S., Gonzalez, L. E., Mandell, J. D., Mane, S. M., Murtha, M. T., Sullivan, C. A., Walker, M. F., Waqar, Z., Wei, L., Willsey, A. J., Yamrom, B., Lee, Y. H., Grabowska, E., Dalkic, E., Wang, Z., Marks, S., Andrews, P., Leotta, A., Kendall, J., Hakker, I., Rosenbaum, J., Ma, B., Rodgers, L., Troge, J., Narzisi, G., Yoon, S., Schatz, M. C., Ye, K., McCombie, W. R., Shendure, J., Eichler, E. E., State, M. W., and Wigler, M. (2014) The contribution of de novo coding mutations to autism spectrum disorder. *Nature* **515**, 216–221

35. Sanders, S. J., Murtha, M. T., Gupta, A. R., Murdoch, J. D., Raubeson, M. J., Willsey, A. J., Ercan-Sencicek, A. G., DiLullo, N. M., Parikshak, N. N., Stein, J. L., Walker, M. F., Ober, G. T., Teran, N. A., Song, Y., El-Fishawy, P., Murtha, R. C., Choi, M., Overton, J. D., Bjornson, R. D., Carriero, N. J., Meyer, K. A., Bilguvar, K., Mane, S. M., Sestan, N.,

Lifton, R. P., Günel, M., Roeder, K., Geschwind, D. H., Devlin, B., and State, M. W. (2012) De novo mutations revealed by whole-exome sequencing are strongly associated with autism. *Nature* **485**, 237–241

36. Planells-Cases, R., Caprini, M., Zhang, J., Rockenstein, E. M., Rivera, R. R., Murre, C., Masliah, E., and Montal, M. (2000) Neuronal death and perinatal lethality in voltage-gated sodium channel alpha(II)-deficient mice. *Biophys. J.* **78**, 2878–2891

37. Ogiwara, I., Miyamoto, H., Tatsukawa, T., Yamagata, T., Nakayama, T., Atapour, N., Miura, E., Mazaki, E., Ernst, S. J., Cao, D., Ohtani, H., Itohara, S., Yanagawa, Y., Montal, M., Yuzaki, M., Inoue, Y., Hensch, T. K., Noebels, J. L., and Yamakawa, K. (2018) Nav1.2 haplodeficiency in excitatory neurons causes absence-like seizures in mice. *Commun Biol.* **1**, 1–16

38. Yu, T. W., Chahrour, M. H., Coulter, M. E., Jiralerspong, S., Okamura-Ikeda, K., Ataman, B., Schmitz-Abe, K., Harmin, D. A., Adli, M., Malik, A. N., D'Gama, A. M., Lim, E. T., Sanders, S. J., Mochida, G. H., Partlow, J. N., Sunu, C. M., Felie, J. M., Rodriguez, J., Nasir, R. H., Ware, J., Joseph, R. M., Hill, R. S., Kwan, B. Y., Al-Saffar, M., Mukaddes, N. M., Hashmi, A., Balkhy, S., Gascon, G. G., Hisama, F. M., LeClair, E., Poduri, A., Oner, O., Al-Saad, S., Al-Awadi, S. A., Bastaki, L., Ben-Omran, T., Teebi, A. S., Al-Gazali, L., Eapen, V., Stevens, C. R., Rappaport, L., Gabriel, S. B., Markianos, K., State, M. W., Greenberg, M. E., Taniguchi, H., Braverman, N. E., Morrow, E. M., and Walsh, C. A. (2013) Using whole-exome sequencing to identify inherited causes of autism. *Neuron* **77**, 259–273

39. Krumm, N., O'Roak, B. J., Shendure, J., and Eichler, E. E. (2014) A de novo convergence of autism genetics and molecular neuroscience. *Trends Neurosci.* **37**, 95–105

40. Gratten, J., Visscher, P. M., Mowry, B. J., and Wray, N. R. (2013) Interpreting the role of de novo protein-coding mutations in neuro-psychiatric disease. *Nat. Genet.* **45**, 234–238